Progress In Electromagnetics Research C, Vol. 124, 179–196, 2022

A Preference Multi-Objective Optimization Method for Asymmetric External Rotor Switched Reluctance Motor

Chaozhi Huang, Hongwei Yuan*, Yuliang Wu, Yongmin Geng, and Wensheng Cao

Abstract—To improve the performance (low torque ripple, high average torque, and high efficiency) of the external rotor switched reluctance motor (ERSRM), a preference multi-objective optimization framework for design and control of an ERSRM based on CD-NSGA-II (Chi-square distance fast non-dominated sorting genetic algorithm) with gradient targets is investigated. Firstly, the structure of the ERSRM is introduced, and the comprehensive sensitive analysis that evaluates the influence of each design variable on optimization objectives is presented. Secondly, the initialization of population, cross-mutation method, and sorting method of conventional NSGA-II are improved. Then, the practicability of this method was proved by standard test functions. Finally, the NSGA-II and CD-NSGA2-II are combined with the visual basic script (VBS) script to optimize the ERSRM, respectively. Finite-element analysis results confirmed the validity and superiority of the optimized design.

1. INTRODUCTION

As a cost-effective, healthy, and environmental-friendly personal tool of transportation, electric bicycles (E-bikes) are gaining an increasing market share from conventional bicycles and automobiles [1, 2]. Switched resistance motor (SRM) has become an ideal hub drive motor due to its good control drive characteristics, high motor energy density, and system efficiency [3]. However, they also have disadvantages such as high acoustic noise and torque ripple. Nowadays, there is increasing attention on the study of torque pulsation reduction of SRM from the structure and control method [4].

The commonly used method for multi-objective optimization of SRM is to fit the surrogate models between the design variables and the optimization objectives according to the finite element analysis (FEA) experimental data, including the response surface model [5], neural network model [6], Kriging model [7], and support vector machine model [8], and then the optimal solutions of these models can be generated by the optimization algorithm.

Ref. [9] proposes a multi-objective differential evolution (MODE) algorithm combining generalized regression neural network (GRNN) to enhance the performance of ferrite-assisted synchronous reluctance (FASR) motor. The comparison of results of mode with multi-objective genetic algorithm (MOGA) and multi-objective particle swarm optimization (MOPSO) algorithm indicates the suitability of MODE to arrive at optimal solutions. However, some of these solutions may be unacceptable because they are impossible to establish or to analyze in FEA dedicated software even though they are correct and achieve the desired objectives from an analytical point of view. Thus, an accurate optimization method combining multi-objective optimization and multi-physical field electromagnetic computing on different platforms has become a research hotspot. This optimization method interfaces the optimization algorithm with simulation software, and the model parameter values are generated by the optimization algorithm and then passed to the simulation software for FEA. After FEA, the simulation results are

Received 24 June 2022, Accepted 2 September 2022, Scheduled 23 September 2022
* Corresponding author: Hongwei Yuan (2550747126@qq.com).
The authors are with the College of Electrical and Automation, Jiangxi University of Science and Technology, Ganzhou 341000, China.

returned to the algorithm for selection, realizing the optimization closed-loop. Ref. [4] uses MATLAB and MotorSolve to jointly optimize the SRM conversion efficiency, average torque, and torque ripple where the rotor and stator structure parameters and firing angles are defined as the optimization variables. Refs. [8, 10] adopt a closed-loop optimization design method that connects FEA and intelligent algorithm optimizer by the transformation of script files. In this way, each calculation step is a closed loop. The implemented optimizer reshapes the FEA model automatically, and then the FEA simulation results are sent back to optimizer. The traditional multi-objective algorithm first needs to obtain a series of non-dominant solutions on the optimization objectives, and then the solutions that meet the expectations of the decision maker according to the actual needs are selected. The motor optimization time greatly depends on the search efficiency and convergence quality of the selected algorithm because each iteration requires FEA to obtain the experimental data when using the accurate optimization method. Traditional multi-objective evolutionary algorithms treat each objective equally and search randomly in all solution spaces without using preference information. This might reduce the search efficiency and the quality of solutions preferred by decision makers, especially when solving problems with complicated properties or many objectives [11].

To improve the search efficiency and the quality of preferred solutions, some attention [12–14] about incorporating preferences into the search process of multi-objective evolutionary algorithms has been paid recently. Molina et al. [15] proposed a reference point method based on the optimization algorithm, g-NSGA-II, which replaces Pareto dominance relation with a new variant, g-Dominance. However, the algorithm is greatly affected by the reference point setting. If the reference point is unreasonable, the algorithm will not converge. Said et al. [16] extended NSGA-II to r-NSGA-II based on a new variant of Pareto dominance relation, that is, r-Dominance. The proposed algorithm converges faster than the g-NSGA-II algorithm and has smaller requirements for reference point setting. Li et al. [17] proposed an r-MOEA/D-STM (Stable Matching Based Selection in Evolutionary Multi-objective Optimization with reference points) algorithm that applies weight vectors to introduce the decision maker's preference information, and this algorithm selects several weights closest to the reference point set by the decision maker as preference regions. And this algorithm trades off the convergence and diversity of the evolutionary search through a stable matching model. The effectiveness of algorithms has been demonstrated by standard test functions. However, more efforts are needed to demonstrate their effectiveness in real engineering problems, especially in motor optimization problems.

Based on the previous research above, we propose a CD-NSGA-II preference optimization algorithm based on gradient adaptive objectives. The zero-ductility transition (ZDT) and diode-transistor logic with Zener diode (DTLZ) functions are selected to prove the feasibility and effectiveness of the preference algorithm. Then, the FEA and preference algorithm are connected here by the transformation of script files to optimize an asymmetric external rotor switched reluctance motor (ERSRM).

2. STRUCTURE OF THE ERSRM

Figure 1(a) depicts the configuration of the proposed ERSRM with multiple teeth structures. The motor is composed of three phases, and each phase has two concentrated windings. Each stator pole consists of three teeth, and the rotor comprises 20 teeth, so the motor has a 18/20-tooth configuration. The basic parameters of the motor are listed in Table 1.

Table 1. Basic parameters of simulation model.

Items	value	Items	value
Rotor outer diameter (mm)	210	Stator outer diameter (mm)	164
Rotor inner diameter (mm)	165.4	Stator yoke width (mm)	26
Air-gap length (mm)	0.7	Operating voltage (V)	48
Stack length (mm)	50	Current limit value	20
Rated speed (rpm/min)	350	Output power (W)	$< 400\,\mathrm{W}$

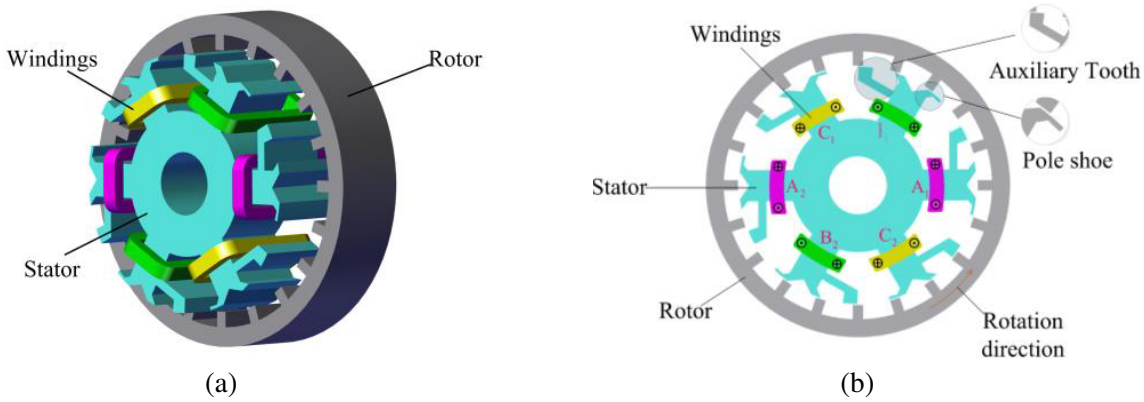

Figure 1. (a) 3-D structure diagram of the ERSRM. (b) 2-D structure diagram of the ERSRM.

3. FLOW OF THE OPTIMIZATION DESIGN

The optimization flowchart is shown in Fig. 2. From the flowchart, the optimization design procedure includes four steps.

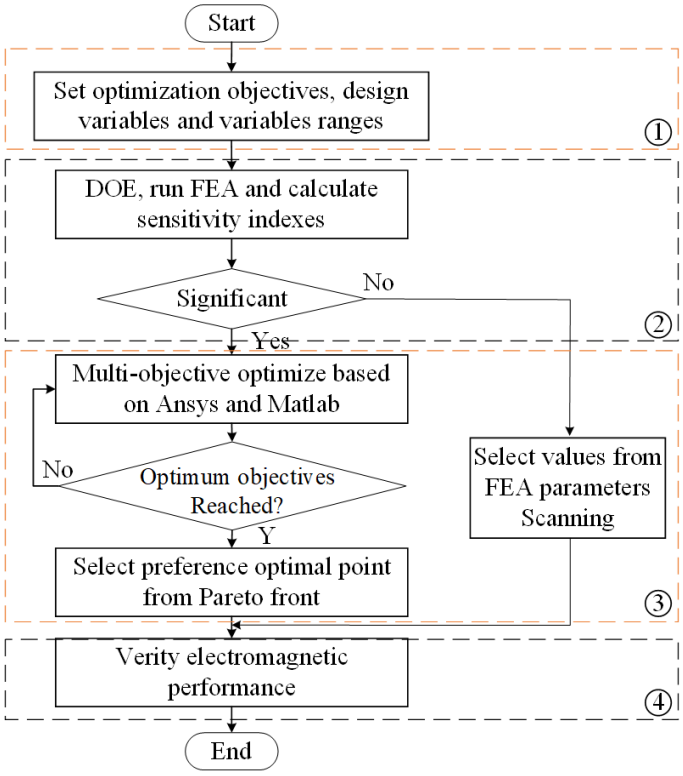

Figure 2. Flowchart of the multi-objective optimization design.

Firstly, the optimization objectives and design variables are determined, and then the sample data are established to analyze the sensitivity index of each design variable to the optimization objectives. As a commonly used scheme in the optimization design process, sensitivity analysis method can screen out the variables that are strongly related to the optimization objectives, thus it can improve the optimization efficiency [18, 19]. The design variables are divided into two categories according to their

significance. The preference algorithm is used to further optimize the significant variables, and the nonsignificant variables are determined by single-parameter scan results. Then, the Pareto front of the optimization objectives will be generated by the preference algorithm. Accordingly, the optimal values of the significant variables can be determined.

3.1. Optimization Objectives and Design Variables

The hub drive motor should have large torque, low torque pulsation, and relatively high efficiency to fit the frequent acceleration and deceleration of electric bicycles in the driving process, as well as the stability and endurance of the driving vehicle. Therefore, torque ripple (T_{rip}), efficiency (η), and the average torque (T_{avg}) are considered as the optimization objectives.

The motor will be simulated at rated condition with limit current of 20 A and reference speed of 350 rpm. T_{rip} is defined as:

$$T_{rip} = \frac{T_{\max} - T_{\min}}{T_{avg}} \times 100\% \tag{1}$$

where $T_{\max}$ and $T_{\min}$ are the highest torque and the lowest torque in one cycle, respectively. T_{avg} is given by:

$$T_{avg} = \frac{1}{t_2 - t_1} \int_{t_1}^{t_2} T dt \tag{2}$$

To facilitate the analysis, only the core loss and stranded loss of ERSRM are considered, and wind and stray loss are not considered. The efficiency of the ERSRM is simply represented as the ratio of the output power to the input power in one cycle.

$$\eta = \frac{P_{out}}{P_{out} + P_{Loss}} \times 100\% \tag{3}$$

$$P_{Loss} = P_{Core\,Loss} + P_{Stranded\,Loss} \tag{4}$$

Based on the output performance and usage of the motor, the initial optimization constraints of ERSRM are set as:

$$\begin{cases} T_{rip} \leq 40\%,\ \eta \geq 80\%, \quad T_{avg} > 7\,\mathrm{N \cdot m} \\ P_{out} + P_{loss} < 400\,\mathrm{W} \end{cases} \tag{5}$$

The ERSRM design variables are selected from motor structure and control parameters. The parameterized cross-section in Fig. 3 includes 11 design parameters, which are rationalized and confined according to Table 2.

Table 2. Design parameters of the ERSRM.

	Parameters	Description	Unit	Range/Value
Structure parameters	N	Windings turns	turns	$30 \sim 50$
	θ_{ps}	Pole shoe angle	mm	$0 \sim 3$
	H_{ps}	Pole shoe height	mm	$0 \sim 3$
	θ_{st1}	Stator tooth 1 angle	deg	$4 \sim 5$
	θ_{st2}	Stator tooth 2 angle	deg	$4 \sim 5$
	θ_{st3}	Auxiliary tooth 3 angle	deg	$5 \sim 9$
	W_1	Auxiliary tooth branch width	mm	$5 \sim 7$
	θ_{mal}	Auxiliary tooth deflection angle	deg	$-3 \sim 1$
	W_{rt}	Rotor tooth width	mm	$6.5 \sim 8.5$
Control parameters	θ_{on}	Turn on angle	deg	$-1 \sim 1$
	θ_{off}	Turn off angle	deg	$6 \sim 9$

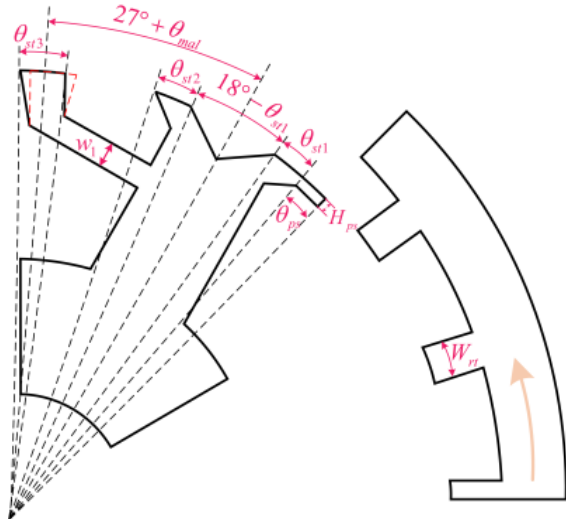

Figure 3. Parameterized model of the studied ERSRM.

3.2. Comprehensive Sensitivity Analysis

After the initial design and the optimized objectives are selected, experimental samples are established by the Latin Hypercube sampling method, and then sample response data are obtained by FEA. Finally, the prediction models of parameters about the optimization objectives based on the sample data are used to evaluate the Pearson correlation coefficient of each design parameter on different design objectives. Pearson correlation coefficient can be given by:

$$\rho_{X_i,Y_i} = \frac{N\sum X_i Y_i - \sum X_i \sum Y_i}{\sqrt{N\sum X_i^2 - (\sum X_i)^2}\sqrt{N\sum Y_i^2 - (\sum Y_i)^2}} \tag{6}$$

where Y_i is the i-th optimization objective, X_i the design parameters, and N the sample size. The sensitivities of all structure and control parameters on the optimization objectives can be calculated based on (6), as shown in Fig. 4. The Pearson correlation coefficients of different optimization objectives are listed in Table 3.

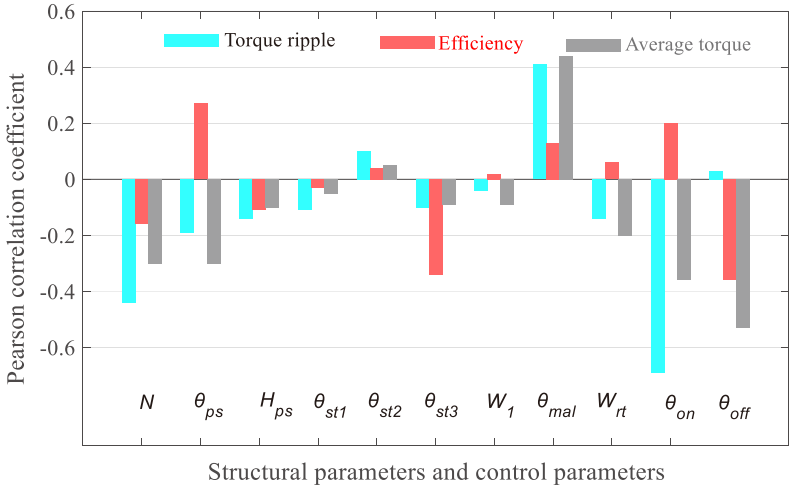

Figure 4. The Pearson correlation coefficient of the structure and control parameters to the three optimization objectives.

Table 3. Pearson correlation coefficients and comprehensive sensitivity indexes of design variables.

Items	$S_{T_{rip}}$ ($w_1 = 0.5$)	S_{η} ($w_1 = 0.25$)	$S_{T_{avg}}$ ($w_1 = 0.25$)	S_{tol}
N	−0.16	−0.30	−0.44	0.27
θ_{ps}	0.27	−0.30	−0.19	0.26
H_{ps}	−0.11	−0.10	−0.14	0.12
θ_{st1}	−0.03	−0.05	−0.11	0.06
θ_{st2}	0.04	0.05	0.10	0.06
θ_{st3}	−0.34	−0.09	−0.10	0.22
W_1	0.02	−0.09	−0.04	0.04
θ_{mal}	0.13	0.44	0.41	0.28
W_{rt}	0.06	−0.20	−0.14	0.12
θ_{on}	0.20	−0.36	−0.69	0.36
θ_{off}	−0.36	−0.53	0.03	0.32

However, because a single design variable has different sensitivities indices for different optimization objectives, selecting the key design variables only through the corresponding correlation coefficient results is difficult. In that, weight coefficients are introduced to calculate the comprehensive sensitivity index of each design variable. A comprehensive sensitivity index $S_{tol}(x_i)$ is defined as:

$$S_{tol}(x_i) = w_1 \cdot \left|S_{T_{rip}}(x_i)\right| + w_2 \cdot |S_{\eta}(x_i)| + w_3 \cdot \left|S_{T_{avg}}(x_i)\right| \tag{7}$$

where $S_{T_{rip}}(x_i)$, $S_{\eta}(x_i)$, and $S_{T_{avg}}(x_i)$ are the sensitivity indices of T_{rip}, η, and T_{avg}, respectively. w_1, w_2, and w_3 are the weights of T_{rip}, η, and T_{avg}, respectively. Considering that the ERSRM's inherent high torque ripple affects the smoothness of torque output and stability of bicycle rack, w_1 is set at 0.5, and w_2 and w_3 are set at 0.25.

The comprehensive sensitivity index of the structure and control parameters for the three optimization objectives can be calculated based on (7), as shown in Table 3.

The design variables are stratified according to the comprehensive sensitivity index. We set a threshold λ, and if $S_{tol}(x_i) \geq \lambda$, x_i is determined as a significant variable related to the optimization objectives, else x_i is determined as a nonsignificant variable related to the optimization objectives. λ here is set to 15%. Therefore, the variables N, θ_{ps}, θ_{st3}, θ_{mal}, θ_{on}, and θ_{off} are determined to be significant variables related to the optimization objectives. And they are selected for the algorithm optimization.

4. CD-NSGA-II

The NSGA-II, based on the dominant relationship proposed by Deb et al. [20], determines the rank level by comparing the dominant relationship between individuals and takes the crowding degree as the basis for sorting the same rank layer. The algorithm adds the championship mechanism and elite retention strategy, which reduce the algorithm complexity and accelerate the convergence speed. The proposed algorithm has good global optimization capability while ensuring the uniformity and diversity of the Pareto frontier. The CD-NSGA-II is improved from the traditional NSGA-II, and we have made the following specific improvements.

4.1. Population Initialization Using the Sobol Sequence

The distribution of the initial individuals in the solution space will greatly affect the convergence speed and optimization accuracy, and the uniform initial individuals are beneficial for improving the performance of the algorithm. Sobol sequence is a type of quasi random sequence with lower disparity

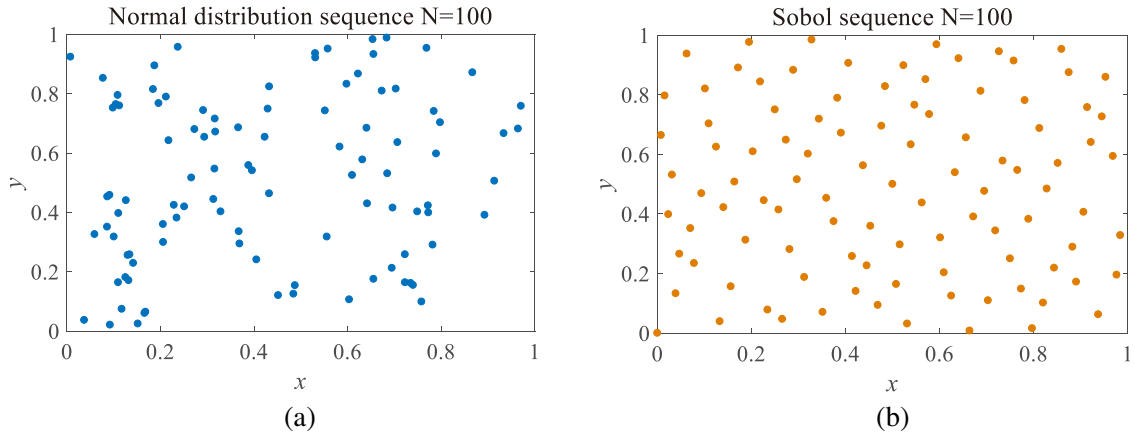

Figure 5. (a) Normal distribution sequence. (b) Sobol sequence.

than the pseudorandom sequence. Using the Sobol sequence for population initializing can keep the population with high diversity [21, 22]. We chose Sobol sequence for the population initialization. Fig. 5 shows a population of 100 in two-dimensional space produced in the range [0, 1], and it shows that the matrix generated by the Sobol sequence is more spatially evenly distributed.

4.2. Normal Crossover and Directional Mutation Strategy

The crossover operator of the conventional NSGA-II adopts the SBX (Simulated binary crossover) operator with poor global search capability and premature convergence of the algorithm. To solve this problem, normal distribution crossover (NDX) operator is proposed. After the parent P_1 and P_2 are determined, the NDX operator is used to find the offspring x_1 and x_2. The location of the crossover is determined by the bit mutation probability t. When $t <= 0.5$, the offspring x_1 and x_2 are given by:

$$\begin{cases} x_{1,i} = \dfrac{P_{1,i} + P_{2,i}}{2} + \dfrac{1.481\,(P_{1,i} - P_{2,i})\,|N\,(0,1)|}{2} \\ x_{2,i} = \dfrac{P_{1,i} + P_{2,i}}{2} - \dfrac{1.481\,(P_{1,i} - P_{2,i})\,|N\,(0,1)|}{2} \end{cases} \tag{8}$$

When $t \geq 0.5$, the offspring x_1 and x_2 are given by:

$$\begin{cases} x_{1,i} = \dfrac{P_{1,i} + P_{2,i}}{2} - \dfrac{1.481\,(P_{1,i} - P_{2,i})\,|N\,(0,1)|}{2} \\ x_{2,i} = \dfrac{P_{1,i} + P_{2,i}}{2} + \dfrac{1.481\,(P_{1,i} - P_{2,i})\,|N\,(0,1)|}{2} \end{cases} \tag{9}$$

where $|N(0,1)|$ is the normal distributed random variable. The crossover operator adopts the NDX operator, improving the ergodic of the solution space and enhancing the global search capability of the algorithm.

The mutation operator of the conventional NSGA-II adopts the polynomial mutation. The location of the mutation is determined by the bit mutation probability P_m. When a random number m is randomly produced, if $m > P_m$, the mutation occurs at that location. In order to ensure that the algorithm can evolve in the direction of optimization, we propose an optimization strategy for directional mutation. The six variables and three-objective optimization of the ERSRM is taken as a case study. The specific operation is as follows:

Firstly, three individuals containing optimal values on each optimization objective in the population of the current evolutionary are selected, and the differences in six individual genes are compared. The formula for calculating the genetic difference is given by:

$$\sigma = \frac{\sum_{j}^{n} |x_i(j) - \overline{x_i}\,|}{n} \tag{10}$$

where n is the number of optimization objectives; $x_i(j)$ is the i-th gene of individual j; $\overline{x_i}$ is the mean of the i-th genes of the three selected individuals.

Secondly, the threshold α is set. If $\sigma < \alpha$, the algorithm distinguishes the gene as a non-differentially expressed gene that causes individual differences, else the gene is distinguished as a differentially expressed gene that causes individual differences. For non-differentially expressed gene, the offspring gene takes a value within the range of the maximum and minimum values expressed by the three selected parents. For a differentially expressed gene, the offspring gene selects a random number within the range of value allowed by the gene. The mutation mode is shown in Fig. 6.

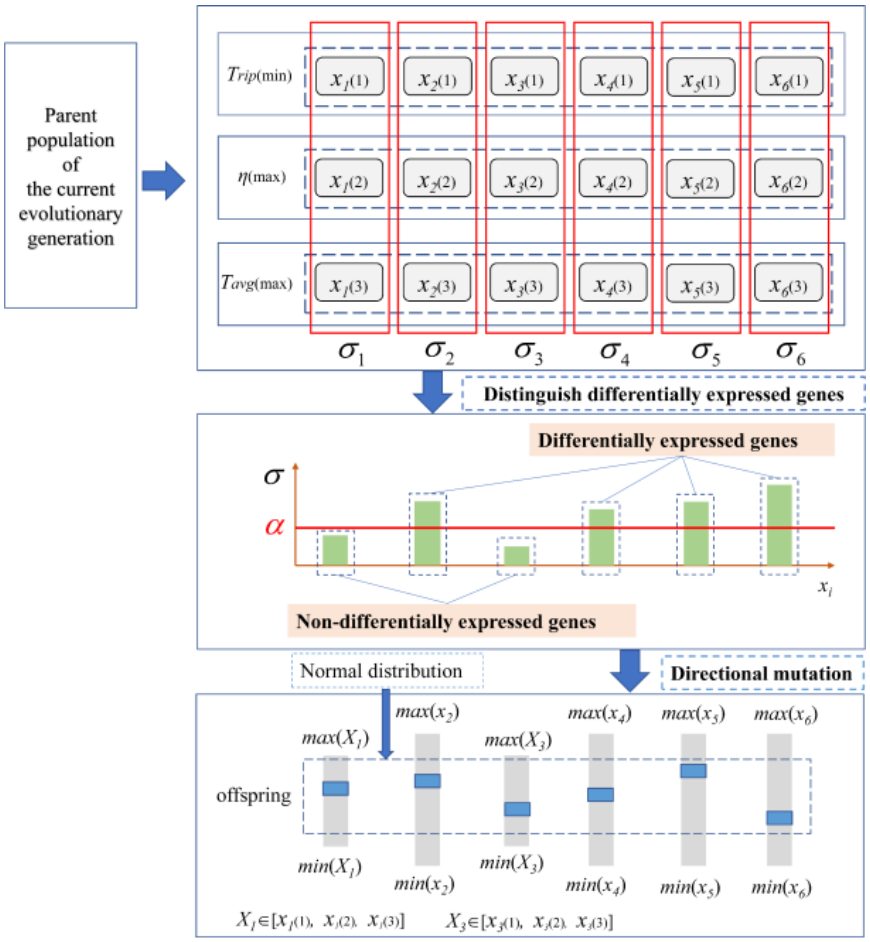

Figure 6. Schematic diagram of directional mutation.

4.3. Sort of the Weighted Chi-Square Distance Based on Adaptive Gradient Targets

Chi-square distance has been widely used in the field of pattern recognition and image processing, as a kind of important information to measure the similarity between two individuals [23, 24]. Chi-square distance formula can be given by:

$$d(x, y) = \sum_{i=1}^{n} \frac{(x_i - y_i)^2}{x_i + y_i} \tag{11}$$

where $d(x, y)$ is the weighted Chi-square distance of solution x to the reference point y; n is the dimension of solution x; x_i and y_i are the value on the i-th dimension of x and y, respectively.

Based on the traditional NSGA-II, we choose the comprehensive weighted Chi-square distance between the individual and the gradient evolutionary targets to replace the traditional NSGA-II

crowding operator, and it is used as a secondary merit criterion reserved for elites in the NSGA-II algorithm championship.

The basic search steps of CD-NSGA-II are like NSGA-II: the non-dominated sorting is applied to classify the combined population individuals into different levels of non-domination. Solutions selected from subsequent non-dominated fronts in the order of their level ranking are kept as candidates, from which the next generation population are chosen by the Chi-square distance operator. In CD-NSGA-II, the shorter the weighted Chi-square distance is between the solution and gradient evolutionary targets, the more likely it is to be preserved for the next generation.

The gradient evolutionary targets setting takes the union of the optimal values on each optimization target in the population of the current evolutionary as the basic evolutionary target, and then sets the step value of each target and progresses step by step. The rank coefficient is then assigned according to the difficulty of each optimization target, and the comprehensive weighted Chi-square distance between the solution to each evolutionary target is calculated.

The ERSRM optimization is taken as a case study. Assume that the optimal solution is $[T_{rip}(\min), \eta(\max), T_{avg}(\max)]$ in the population of the current evolutionary. The gradient evolution targets values are set as:

$$\begin{cases} \text{Target}\,(1) = [T_{rip}\,(\min)\,, \eta\,(\max)\,, T_{avg}\,(\max)] \\ \text{Target}\,(2) = [T_{rip}\,(\min) + \Delta T_{rip}, \eta\,(\max)\,, T_{avg}\,(\max)] \\ \text{Target}\,(3) = [T_{rip}\,(\min) + \Delta T_{rip}, \eta\,(\max) + \Delta\eta, T_{avg}\,(\max)] \\ \text{Target}\,(4) = [T_{rip}\,(\min) + \Delta T_{rip}, \eta\,(\max) + \Delta\eta, T_{avg}\,(\max) + \Delta T_{avg}] \\ \text{Target}\,(5) = [T_{rip}\,(\min) + 2\Delta T_{rip}, \eta\,(\max) + \Delta\eta, T_{avg}\,(\max) + \Delta T_{avg}] \end{cases} \tag{12}$$

where ΔT_{rip}, $\Delta\eta$, and ΔT_{avg} are the step value on T_{rip}, η and T_{avg}, respectively. Here ΔT_{rip}, $\Delta\eta$, and ΔT_{avg} are set to 1%, 1%, and 0.5 N·m, respectively.

Then, the comprehensive weighted Chi-square distance between the individual j and the gradient evolutionary targets can be given by:

$$d(i) = \sum_{k=1}^{5} \omega_k \cdot \sum_{m=1}^{3} \lambda_m \cdot \left((f_m(i) - \text{Target}(k)_m)^2 / (f_m(i) - \text{Target}(k)_m) \right) \tag{13}$$

where k is the gradient evolutionary target number; m is the individual optimization target value number; $f_m(i)$ is the m-th optimization target value of the individual i; $\text{Target}(k)_m$ is the m-th optimization target value of the k-th gradient evolutionary target; w_k is the rank coefficient of gradient k-th evolutionary target; and λ_m is the weight for the m-th evolutionary target value. $\omega_1 \sim \omega_5$ are set to be 1, 2, 3, 6, and 12, respectively. It means that the higher-level target has higher priority than the previous targets. The weight coefficients λ_1, λ_2, and λ_3 are determined at 0.5, 0.25, and 0.25 according to the optimize preferences, respectively.

The flowchart of ERSRM optimization based on CD-NSGA-II is in Fig. 7.

5. CD-NSGA-II TEST

To prove the feasibility of local optimization of the proposed algorithm and the effectiveness of the improvement strategy and objective preference, we used the two-objective ZDT1 functions and three-objective DTLZ4 functions. We select the inverted generational distance based on the composite front (IGD-CF), which was proposed by Mohammadi et al. [25] to analyze the effect of different strategies on the convergence of the proposed algorithm. The metric defined a region of interest (ROI) based on the location of a user-supplied reference point. It uses a composite front which is a type of reference set, and it is used as a replacement for the Pareto-optimal front. Then the classic inverted generational distance (IGD) [26] is calculated in this ROI. IGD-CF can be obtained as:

$$IGD - CF\,(P_{ROI}, PF_{ROI}) = \frac{\sum_{x \in PF_{ROI}} d\,(x, P_{ROI})}{|PF_{ROI}|} \tag{14}$$

where P_{ROI} are the obtained solutions in the ROI; PF_{ROI} are the real composite front solutions in the ROI; $d(x, P_{ROI})$ is the closest Euclidean distance of sample points in the PF_{ROI} to the obtained solutions in the P_{ROI}.

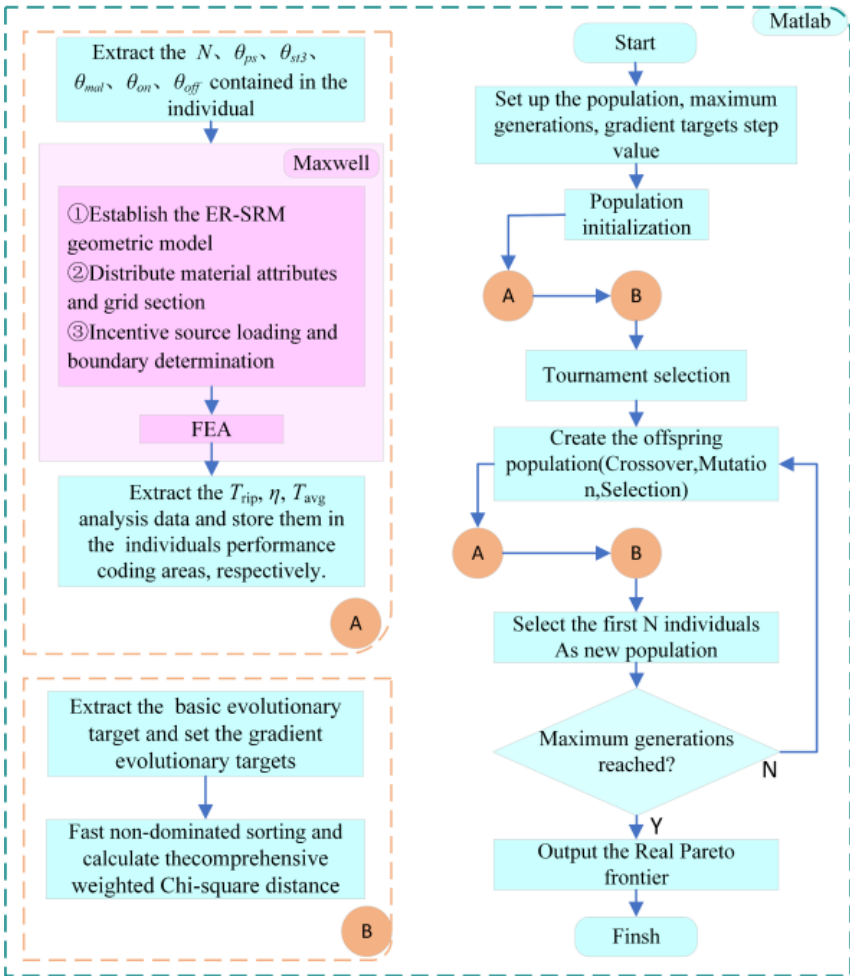

Figure 7. Flowchart of ERSRM optimization based on CD-NSGA-II.

5.1. Two-Objective Test Problems

The double-objective ZDT1 test problem is taken as a case study. The population size is set to 100 for ZDT1, and the number of iterations in each run is 50.

We used [0.2, 0.55] as the reference point for ZDT1. To specify the size of the ROI on the Pareto-optimal front of ZDT1, the radius of ROI is set to 0.02. Under the same population and the number of iterations, the mean IGD-CF of 10 independent runs is obtained with different population initializing modes. Fig. 8 shows the change curves of IGD-CF under different population initializing modes.

It can be seen from Fig. 8 that the algorithm convergence speed is significantly improved after using the Sobol sequence on the ZDT1 problem.

Under the same population and the number of iterations, the mean IGD-CF of 10 independent runs is obtained with different cross-mutation strategies and same Sobol sequence population initializations. Fig. 9 shows the change curves of IGD-CF under different cross-mutation strategies.

Figure 9 shows that the algorithm using normal crossover and directional mutation has better convergence result than the algorithms with simulated binary crossover and polynomial mutation before the 31st generation.

We use [0.2, 0.55] and [0.4, 0.4] as the reference points for the Chi-square distance calculation. When the coefficients of the two reference points are set to 1&1, 1&3, 3&1, respectively, the Preto frontier distributions after the algorithm iterations are shown in Fig. 10, respectively.

It can be seen from Fig. 10 that when the coefficients of the two reference points are equal, the

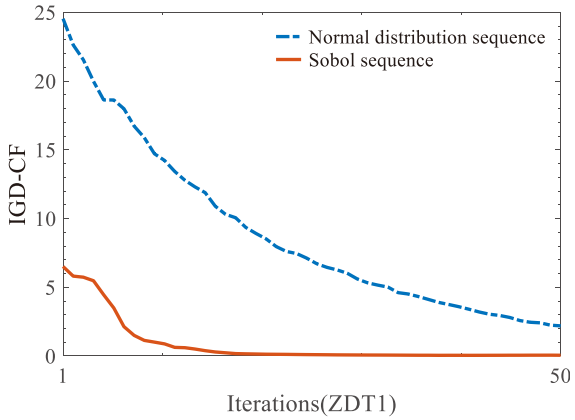

Figure 8. Comparison of IGD-CF under different population initializing modes.

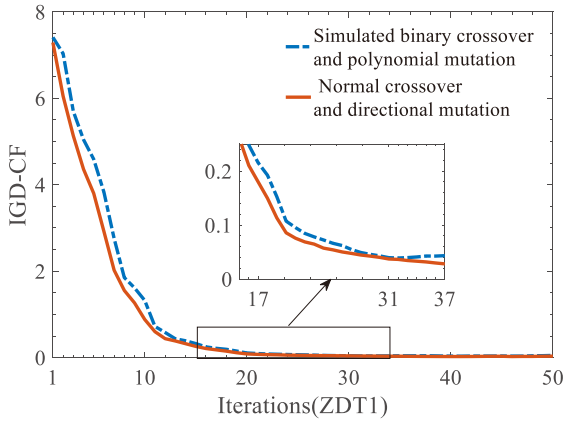

Figure 9. Comparison of IGD-CF under different cross-mutation strategies.

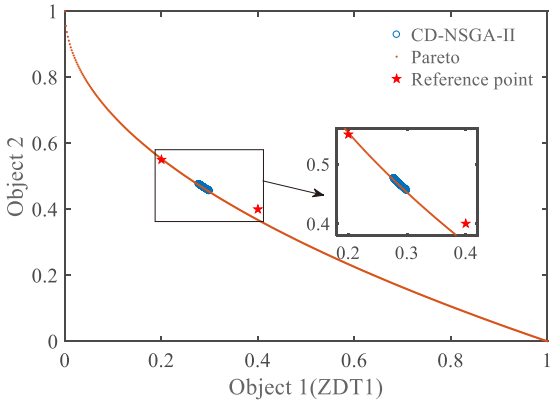

(a)

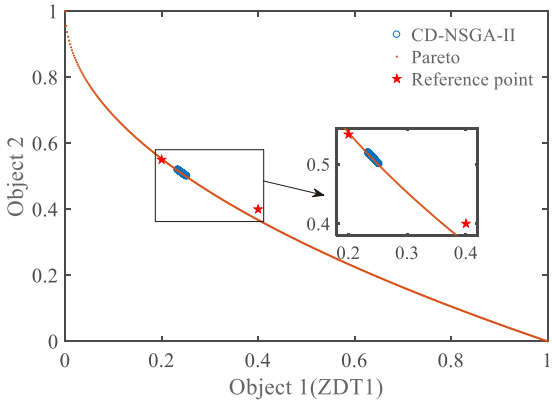

(b)

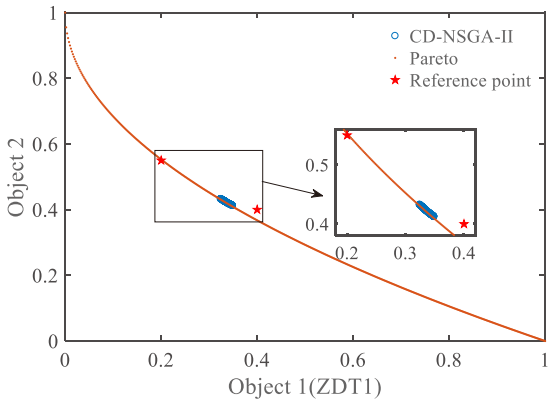

(c)

Figure 10. (a) The coefficients of the two reference points are equally. (b) The coefficient of [0.2, 0.55] is higher. (c) The coefficient of [0.4, 0.4] is higher.

algorithm convergence area is in the middle area of the two reference points. When the coefficients of the two reference points are different, the algorithm convergence region moves to the reference point with a higher coefficient.

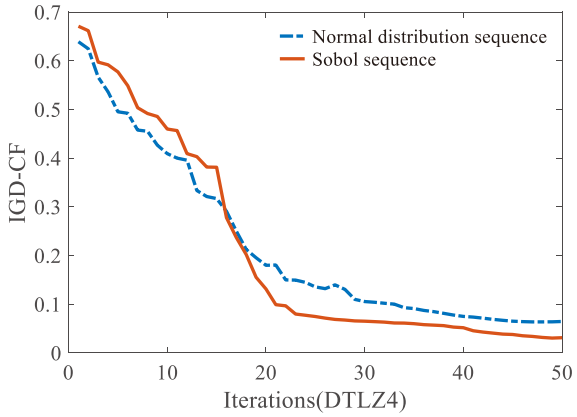

Figure 11. Comparison of IGD-CF under different population initializing modes.

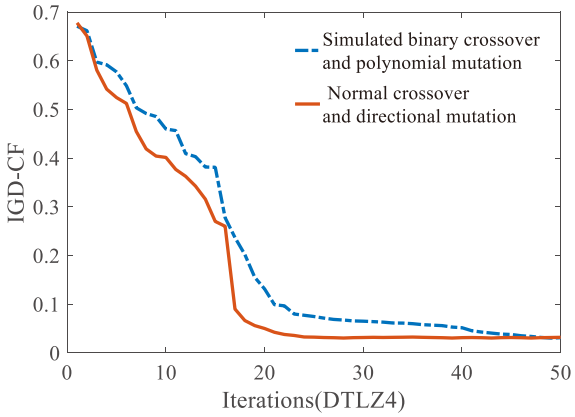

Figure 12. Comparison of IGD-CF under different cross-mutation strategies.

5.2. Three-Objective Test Problems

The three-objective test problem is taken as a case study. The population size is set to 100 for DTLZ4, and the number of iterations in each run is 50.

We use [0.5, 0.5, 0.7] as the reference point for DTLZ4. To specify the size of the ROI on the

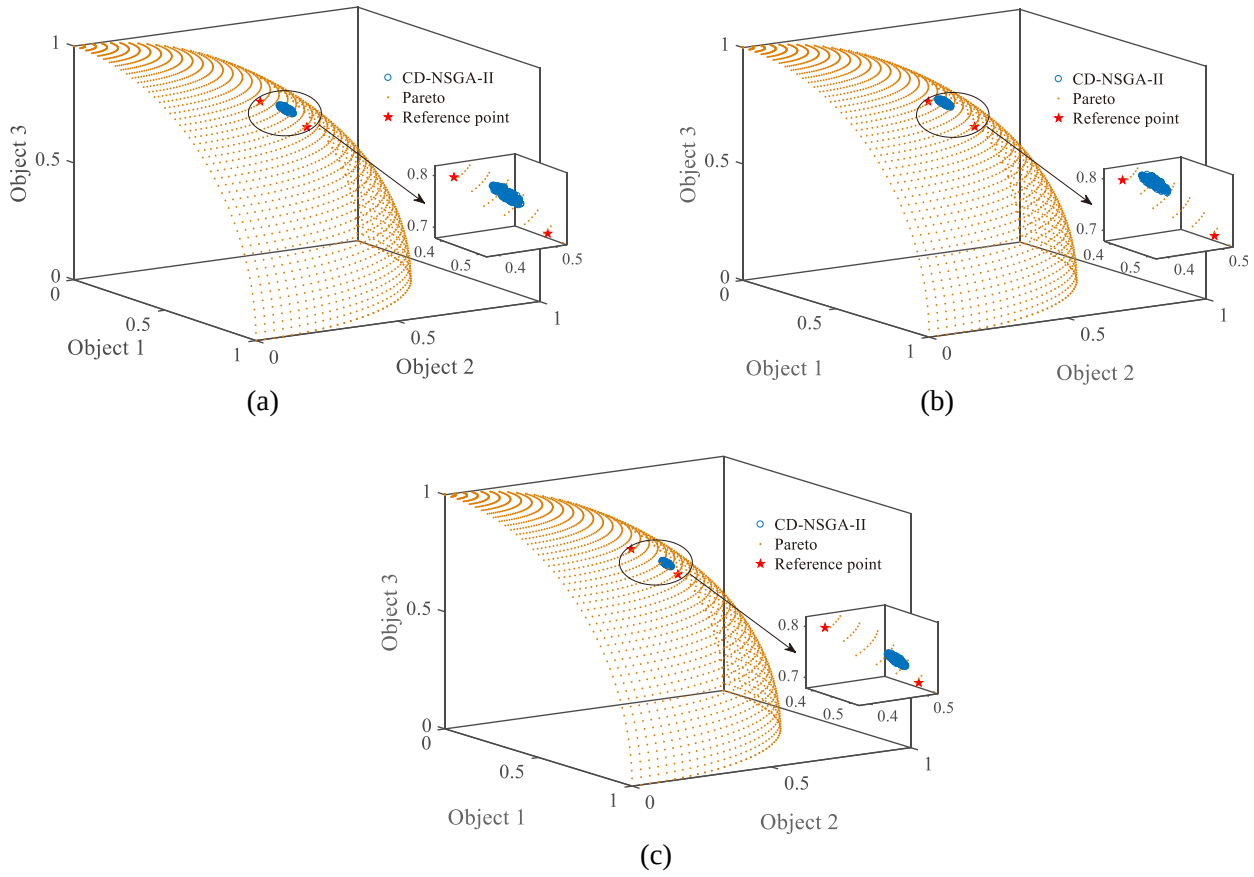

Figure 13. (a) The two reference points with equally coefficient. (b) [0.4, 0.4, 0.8] coefficient is higher. (c) [0.5, 0.5, 0.7] coefficient is higher.

Pareto-optimal front of DTLZ4, the radius of ROI is set to 0.1. Under the same population and the number of iterations, the mean IGD-CF of 10 independent runs is obtained with different population initializing modes. Fig. 11 shows the change curves of IGD-CF under different population initializing modes.

It can be seen from Fig. 11 that the algorithm using the Sobol sequence has bigger IGD values than the algorithm using the normal distribution sequence before 16th iteration, which means that the solution set distribution is more dispersed in the early iteration of the algorithm using the Sobol sequence. After the 16th generation, the IGD value of the algorithm using the Sobol sequence is always lower than the algorithm using the normal distribution sequence.

Under the same population and the same number of iterations, the mean IGD-CF of 10 independent runs is obtained with different cross-mutation strategies and the same Sobol sequence population initialization. Fig. 12 shows the change curves of IGD-CF under different cross-mutation strategies.

Figure 12 shows that the algorithm using normal crossover and directional mutation has better convergence result than the algorithm with simulated binary crossover and polynomial mutation.

We use [0.5, 0.5, 0.7] and [0.4, 0.4, 0.8] as the reference points for the Chi-square distance calculation. When the coefficients of the two reference points are set to 1&1, 1&3, 3&1, respectively, the Preto frontier distributions after the algorithm iterations are shown in Fig. 13, respectively.

It can be seen from Fig. 13 that when the coefficients of the two reference points are equal, the algorithm convergence area is in the middle area of the two reference points. When the coefficients of the two reference points are different, the algorithm convergence region moves to the reference point with a higher coefficient.

To sum up, it can be seen that the main CD-NSGA-II search area and algorithm convergence domain will change accordingly with the reference point selection. When the grade coefficients of the reference points are different, the algorithm convergence area will move to the reference point with a higher coefficient. Therefore, we can obtain optimal solutions by setting gradient evolutionary targets to make the population evolve in a better direction.

6. COMPARISON OF PARETO OPTIMAL SOLUTIONS AND SIMULATION VERIFICATION

Based on the above experiments, we select NSGA-II and CD-NSGA-II combined with VBS script to optimize the ERSRM. The main parameters of NSGA-II and CD-NSGA-II are listed in Table 4.

The optimization results for NSGA2 and CD-NSGA-II are shown in Fig. 14(a) and Fig. 14(b), respectively. The color maps illustrate the progression of the search; the final population is illustrated in red.

From Fig. 14, we can conclude that the NSGA-II is biased toward global convergence, while the

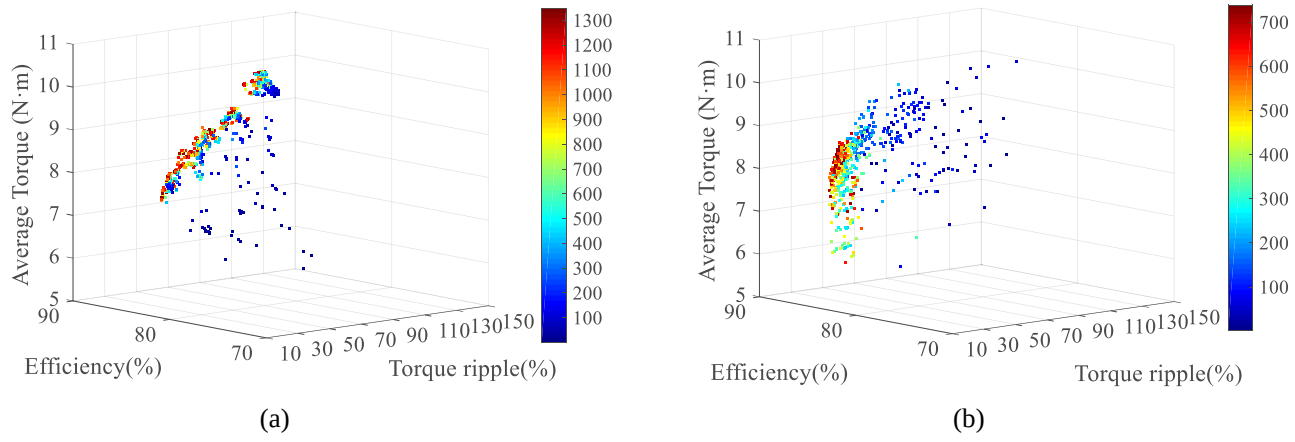

Figure 14. (a) Optimization objectives results for all studied points of NSGA-II. (b) Optimization objectives results for all studied points of CD-NSGA-II.

Table 4. The main parameters of NSGA-II & CD-NSGA-II.

Parameters	NSGA-II	CD-NSGA-II
Population	30	30
Max iterations	50	30
Crossover coefficient	0.8	0.8
Mutation coefficient	0.2	0.2

CD-NSGA-II is more inclined to local convergence.

The value function is given by:

$$\begin{cases} u(T_{rip},\eta,T_{avg}) = \lambda_1\left(-\dfrac{T_{rip}-\min(T_{rip})}{\max(T_{rip})-\min(T_{rip})}\right)+\lambda_2\dfrac{\eta-\min(\eta)}{\max(\eta)-\min(\eta)}+\lambda_3\dfrac{T_{avg}-\min(T_{avg})}{\max(T_{avg})-\min(T_{avg})} \\ \sum_{i=1}^{3}\lambda_i = 1 \end{cases} \tag{15}$$

where $u(T_{rip},\eta,T_{avg})_{\max}$ is determined as the global optimal solution of the Pareto front solution. The weight coefficients are determined as $\lambda_1 = 0.5$, $\lambda_2 = 0.25$, and $\lambda_3 = 0.25$ according to the priority of the optimization objective.

The weighted solutions of the optimized design in the obtained Pareto solution of NSGA-II and

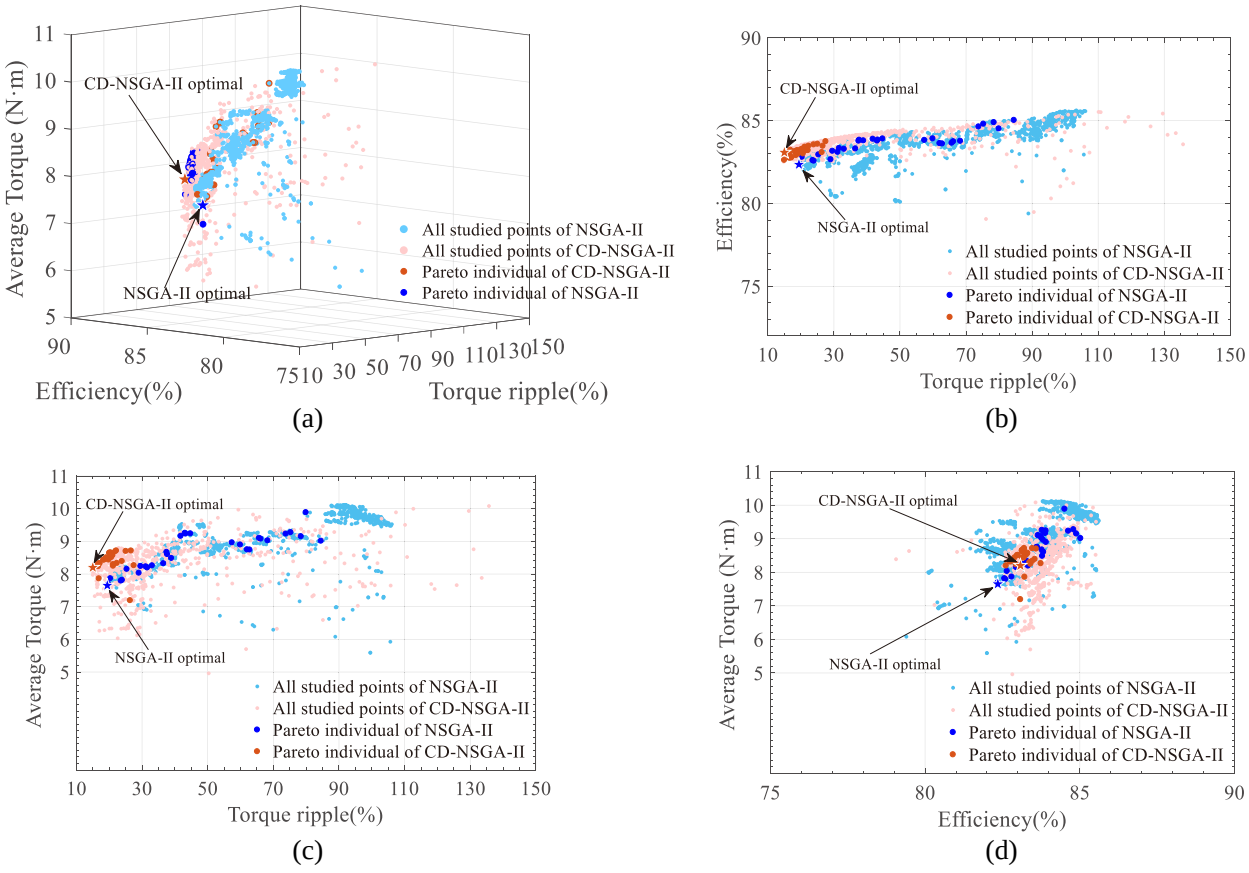

Figure 15. Pareto frontier. (a) 3-D Pareto frontier of NSGA-II and CD-NDGA-II. (b) Torque ripple versus efficiency. (c) Torque ripple versus average torque. (d) Efficiency versus average torque.

Table 5. Design variables and performance of initial and optimal.

	Parameters	Initial	NSGA-II optimal	CD-NSGA-II optimal
Motor parameters	N	38	39	41
	θ_{ps} (◦)	1	2.2	2.4
	H_{ps} (mm)	1.5	1.5	1.5
	θ_{st1} (◦)	4.5	4.5	4.5
	θ_{st2} (◦)	4.5	4.5	4.5
	θ_{st3} (◦)	5	7.95	8.48
	W_1 (mm)	5.6	5.6	5.6
	θ_{mal} (◦)	−1	−2.41	−2.35
	W_{rt} (mm)	7.2	7.2	7.2
	θ_{on} (◦)	0	−0.9	−1
	θ_{off} (◦)	6	7.6	7.5
Output performance	$P_{core\,loss}$ (W)	25.56	32.98	33.21
	$P_{stranded\,loss}$ (W)	19.35	27.11	28.04
	T_{rip} (%)	144.67	19.41	14.99
	η (%)	85.78	82.35	83.07
	T_{avg} (N · m)	7.39	7.65	8.20

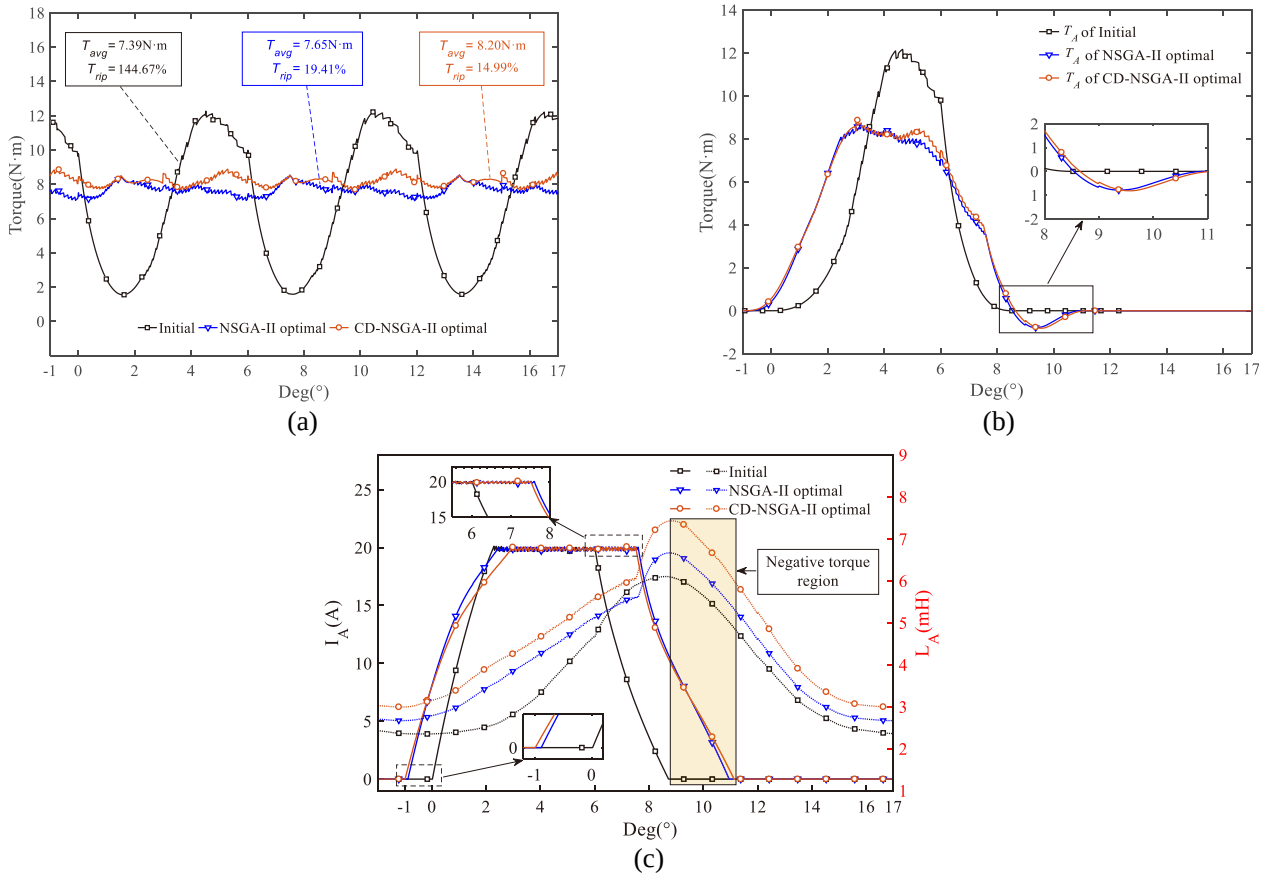

Figure 16. (a) Comparison of transient torque. (b) Comparison of single-phase torque. (c) Comparison of single-phase current with inductance.

CD-NSGA-II are selected by (15), as shown in the blue and brown pentagram in Fig. 15, and the specific parameters of the weighted solutions are shown in Table 5.

Figure 15 shows that torque ripple is positively correlated with efficiency and average torque, which means that pursuing lower torque ripple will lose a part of the average torque and efficiency.

It can be seen from Table 5 that although the optimized motor of CD-NSGA-II efficiency has decreased by 3.16% from 85.78% to 83.07%, the average torque has increased from 7.20 N·m increased by 10.96% to 8.20 N·m, the torque ripple decreased by 89.64% from 144.67% to 14.99% compared with the motor of the initial design, and the torque ripple was significantly reduced. Meanwhile, the torque ripple of the optimized motor of CD-NSGA-II was decreased by 22.93%, the efficiency improved by 0.87%, and the average torque increased by 7.19% compared with the out performance of the optimized motor of NSGA-II. From the 2-D projection of the optimization objectives, CD-NSGA-II can better handle optimization preferences; the scheme is more optional; and the calculation amount is only 55% of NSGA-II.

Figure 16(a), Figure 16(b), Figure 16(c) show the comparison of transient torque, comparison of single phase torque, and comparison of single-phase current with inductance, respectively.

It is worth noting that, after the θ_{off} delay of the motor of the optimization schemes, the single-phase current still does not drop to zero in the inductance drop area, producing a part of negative torque, but the overall synthetic torque is smoother. It means that the starting performance of the motor is improved.

7. CONCLUSION

This paper introduces a preference multi-objective optimization framework for the design and control of an ERSRM based on CD-NSGA-II. We have proved the feasibility of preference optimization of the proposed algorithm and the effectiveness of the proposed strategy by ZDT and DTLZ functions. We combine the algorithm with FEA through VBS script to optimize the asymmetric structure ERSRM. The experimental results show that the CD-NSGA-II algorithm has faster convergence speed and convergence quality than the traditional NSGA-II. It achieves a better optimization effect than the traditional NSGA-II algorithm when the calculation amount is only 55% of the traditional NSGA-II algorithm. Therefore, the proposed optimization design for the ERSRM can obtain the optimal stator and rotor structure design conveniently and efficiently.

ACKNOWLEDGMENT

This work was supported by the National Natural Science Foundation of China under Project 52167005.

REFERENCES

1. Brock, H., B. Berker, and E. Ali, "Design of an external-rotor direct drive E-bike switched reluctance motor," *IEEE Transactions on Vehicular Technology*, Vol. 69, No. 3, 2552–2562, 2020.
2. Lin, J. N., N. Schofield, and E. Ali, "External-rotor 6–10 switched reluctance motor for an electric bicycle," *IEEE Transactions on Transportation Electrification*, Vol. 1, No. 4, 348–356, 2015.
3. Berker, B., H. Brock, D. Alan, et al., "Making the case for switched reluctance motors for propulsion applications," *IEEE Transactions on Vehicular Technology*, Vol. 69, No. 7, 7172–7186, 2020.
4. Anvari, B., H. A. Toliyat, and B. Fahimi, "Simultaneous optimization of geometry and firing angles for in-wheel switched reluctance motor drive," *Current Forestry Reports*, Vol. 4, No. 1, 322–329, 2018.
5. Ma, C. and L. Y. Qu, "Multiobjective optimization of switched reluctance motors based on design of experiments and particle swarm optimization," *IEEE Transactions on Energy Conversion*, Vol. 30, No. 3, 1144–1153, 2015.
6. Zhang, Z., S. H. Rao, and X. Zhang, "Performance prediction of switched reluctance motor using improved generalized regression neural networks for design optimization," *China Electrotechnical Society Transactions on Electrical Machines and Systems*, Vol. 2, No. 4, 371–376, 2018.

7. Xia, B., Z. Ren, Y. L. Zhang, and C. Koh, "An adaptive optimization algorithm based on kriging interpolation with spherical model and its application to optimal design of switched reluctance motor," *Journal of Electrical Engineering and Technology*, Vol. 9, No. 5, 1544–1550, 2014.
8. Hua, Y. Z., H. Q. Zhu, M. Gao, and Z. Ji, "Multi-objective optimization design of permanent magnet assisted bearingless synchronous reluctance motor using NSGA-II," *IEEE Transactions on Industrial Electronics*, Vol. 68, No. 11, 10477–10487, 2020.
9. Nagarajan, V. S., B. Mahadevan, V. Kamaraj, et al., "Design optimization of ferrite assisted synchronous reluctance motor using multi-objective differential evolution algorithm," *The International Journal for Computation and Mathematics in Electrical and Electronic Engineering*, Vol. 36, No. 1, 219–239, 2017.
10. Mohamed, E., A. Mohamed, R. Hegazy, and N. I. Mohamed, "Finite element based overall optimization of switched reluctance motor using multi-objective genetic algorithm (Nsga-II)," *Mathematics*, Vol. 9, No. 5, 1–20, 2021.
11. Rong, T., L. Ke, D. Wei, Y. T. Wang, et al., "Reference point based multi-objective optimization of reservoir operation: A comparison of three algorithms," *Water Resources Management*, Vol. 34, No. 3, 1005–1020, 2020.
12. Hu, J., G. Yu, J. H. Zheng, and J. Zou, "A preference-based multi-objective evolutionary algorithm using preference selection radius," *Soft Computing — A Fusion of Foundations, Methodologies & Applications*, Vol. 21, No. 17, 5025–5051, 2017.
13. Wang, L. P., M. L. Zhang, F. Y. Qiu, and B. Jiang, "Many-objective optimization algorithm with preference based on the angle penalty distance elite selection strategy," *Jisuanji Xuebao/Chinese Journal of Computers*, Vol. 41, No. 1, 236–253, 2018.
14. Wang, S. F., J. H. Zheng, J. J. Hu, J. Zou, and G. Yu, "Multi-objective evolutionary algorithm for adaptive preference radius to divide region," *Journal of Software*, Vol. 28, No. 10, 2704–2721, 2017.
15. Molina, J., L. V. Santana, A. G. Hernandez-Diaz, C. A. Coello Coello, and R. Caballero, "g-dominance: Reference point based dominance for multiobjective metaheuristics," *European Journal of Operational Research*, Vol. 197, No. 2, 685–692, 2009.
16. Said, B. L., S. Bechikh, and K. Ghedira, "The r-dominance: A new dominance relation for interactive evolutionary multicriteria decision making," *IEEE Transactions on Evolutionary Computation*, Vol. 14, No. 5, 801–818, 2010.
17. Li, K., Q. Zhang, S. Kwong, M. Li, and R. Wang, "Stable matching-based selection in evolutionary multiobjective optimization," *IEEE Transactions on Evolutionary Computation*, Vol. 18, No. 6, 909–923, 2014.
18. Lei, G., C. Liu, J. Zhu, and Y. Guo, "Techniques for multilevel design optimization of permanent magnet motors," *IEEE Transactions on Energy Conversion*, Vol. 30, No. 4, 1574–1584, 2015.
19. Lei, G., W. Xu, J. Hu, J. Zhu, Y. Guo, and K. Shao, "Multilevel design optimization of a FSPMM drive system by using sequential subspace optimization method," *IEEE Transactions on Magnetics*, Vol. 50, No. 2, 685–688, 2014.
20. Deb, K., A. Pratap, S. Agarwal, and T. Meyarivan, "A fast and elitist multiobjective genetic algorithm: NSGA-II," *IEEE Transactions on Evolutionary Computation*, Vol. 6, No. 2, 182–197, 2002.
21. Altinoz, O. T., A. E. Yilmaz, and G. W. Weber, "Improvement of the gravitational search algorithm by means of low-discrepancy sobol quasi random-number sequence based initialization," *Advances in Electrical and Computer Engineering*, Vol. 14, No. 3, 55–62, 2014.
22. Navid, A., S. Khalilarya, and M. Abbasi, "Diesel engine optimization with multi-objective performance characteristics by non-evolutionary Nelder-Mead algorithm: Sobol sequence and Latin hypercube sampling methods comparison in DoE process," *Fuel*, Vol. 228, 349–367, 2018.
23. Kumar, A. and S. Devi, "Novel center symmetric local binary pattern and chi square fuzzy c-mean clustering based segmentation in medical imaging technique," *International Journal of Scientific and Technology Research*, Vol. 8, No. 7, 697–705, 2019.

24. Seong, J. H. and D. H. Seo, "Wi-Fi fingerprint using radio map model based on MDLP and euclidean distance based on the Chi squared test," *Wireless Networks*, Vol. 25, No. 6, 3019–3027, 2019.
25. Mohammadi, A., M. N. Omidvar, and X. Li, "A new performance metric for user-preference based multi-objective evolutionary algorithms," *IEEE Congress on Evolutionary Computation: CEC 2013*, Vol. 4, 2564–3418, 2013.
26. Bosman, P. A. N. and D. Thierens, "The balance between proximity and diversity in multiobjective evolutionary algorithms," *IEEE Transactions on Evolutionary Computation*, Vol. 7, No. 2, 174–188, 2003.